Theory of magnetoelectric resonance in two-dimensional $S = 3/2$ antiferromagnet $Ba_2CoGe_2O_7$ via spin-dependent metal-ligand hybridization mechanism

S. Miyahara[1] and N. Furukawa[1,2]

[1] *Multiferroics Project (MF), ERATO, Japan Science and Technology Agency (JST), c/o Department of Applied Physics, The University of Tokyo, 7-3-1 Hongo, Tokyo 113-8656, Japan*

[2] *Department of Physics and Mathematics, Aoyama Gakuin University, 5-10-1 Fuchinobe, Chuo-ku, Sagamihara, Kanagawa 252-5258, Japan*

(Dated: January 20, 2011)

We investigate magnetic excitations in an $S = 3/2$ Heisenberg model representing two-dimensional antiferromagnet $Ba_2CoGe_2O_7$. In terahertz absorption experiment of the compound, Goldstone mode as well as novel magnetic excitations, conventional magnetic resonance at 2 meV and both electric- and magnetic-active excitation at 4 meV, have been observed. By introducing a hard uniaxial anisotropy term $\Lambda(S^z)^2$, three modes can be explained naturally. We also indicate that, via the spin-dependent metal-ligand hybridization mechanism, the 4 meV excitation is an electric-active mode through the coupling between spin and electric-dipole. Moreover, at 4 meV excitation, an interference between magnetic and electric responses emerges as a cross correlated effect. Such cross correlation effects explain the non-reciprocal linear directional dichroism observed in $Ba_2CoGe_2O_7$.

PACS numbers: 75.80.+q, 75.40.Gb, 75.30.Ds, 76.50.+g

Multiferroic materials have attracted both experimental and theoretical interests due to giant magnetoelectric effects [1–3]. Such strong couplings between magnetism and electric polarization (EP) are often realized through spin-dependent EPs. For example, in cycloidal magnets $R\mathrm{MnO_3}$ (R = Tb, Dy, and others), EP flops from $P\|c$ to $P\|a$ by changing a magnetic state from bc to ab cycloidal state through external magnetic fields [4]. Another example is magnetic resonance induced by oscillating electric field, or *electromagnon*, which is observed in an optical spectroscopy at terahertz (THz) frequencies for a variety of multiferroics compounds, e.g., $R\mathrm{MnO_3}$ [5–7] and $\mathrm{CuFe_{1-x}Ga_xO_2}$ [8]. The exchange striction [7, 9] and the spin current [10–12] mechanisms are well known as the origins of such spin-dependent EP.

Spin-dependent metal-ligand hybridization has been proposed as an alternative mechanism [13, 14]. EP along the bond direction $\mathbf{r}_{ml}$ connecting metal and ligand depends on a spin structure at a metal site $\mathbf{S}_m$ in a form $\mathbf{p}_{ml} \propto (\mathbf{S}_m \cdot \mathbf{r}_{ml})^2 \mathbf{r}_{ml}$. At a spin site with no inversion, such a mechanism can induce an electric dipole which is coupled to the spin, and has a potential to induce novel features. In fact, magnetic field dependence of the ferroelectricity observed in $Ba_2CoGe_2O_7$ can well be explained by introducing this mechanism [15].

$Ba_2CoGe_2O_7$ is a quasi two-dimensional antiferromagnet (Fig. 1 (a)). Below $T_N = 6.7$ K, Co magnetic moments ($S = 3/2$) show an antiferromagnetic structure, where magnetic moments are aligned in xy-plane due to an easy-plane anisotropy [16]. In the magnetically ordered state, peculiar magnetoelectric behaviors have been observed [15, 17]. For example, EP along [001] shows sinusoidal angular dependence with a period of π for a rotation of the magnetic field $\mathbf{B}^{\mathrm{ex}}$ within xy-plane at $B^{\mathrm{ex}} \gtrsim 1$ T. As shown in Ref. 15, such magnetoelectric behaviors can well be explained by a local electric dipole moment which couples to the local spin structure of Co atom via the metal-ligand hybridization mechanism between Co and O atoms. For a classical spin within the xy-plane $\mathbf{S}_m = (S\cos\theta, S\sin\theta, 0)$, an EP on a $\mathrm{CoO_4}$ tetrahedron along z is described as $p_m^z = -S^2 K \cos 2\theta$, which reproduces the experimental results.

However, there still exist several features to be understood. One of them is magnetic excitation property observed in an electromagnetic wave (EMW) absorption experiment (AE) in the THz frequency regime, which indicates magnetic resonances at $\omega \sim 0$ [18], 2, and 4 meV [19]. The lowest two peaks can be assigned to spin wave branches which have been reported in the inelastic neutron scattering experiments (INS) [16]. Here, two distinct modes exist at the Γ point in the two-sublattice ground state due to an anisotropy. However, the origin of the excitation at $\omega \sim 4$ meV is not clear within magnon pictures. The other point to be understood is the THz AE on several EMW polarizations which indicates that the excitation at 4 meV is induced by both magnetic and electric components of EMW, whereas the excitation at 2 meV is excited mainly by the in-plane magnetic component. Moreover, the resonance at 4 meV shows a non-reciprocal directional dichroism (NDD) under the external magnetic fields [19], i.e., absorption intensity strongly depends on the EMW propagation directions (forward $+\mathbf{k}$ or backward $-\mathbf{k}$). In contrast, NDD is not clearly observed at the 2 meV resonance. The origin of the magnetic excitation and the absorption mechanism is very important to understand the principle of the NDD.

In this Letter, we propose that a uniaxial anisotropy term $\Lambda(S_m^z)^2$ ($\Lambda > 0$) gives clues to understand these features. In an $S = 3/2$ system, the uniaxial anisotropy

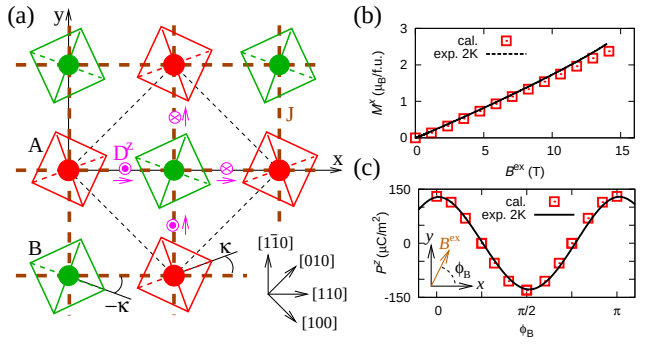

FIG. 1: (Color online) (a) Crystal structure for $Ba_2CoGe_2O_7$. Top view of CoO_4 tetrahedra is illustrated by squares. An $S = 3/2$ spin locates on a Co-site with a spin interaction J. DM interaction $-D^z_{ij}\,(S^x_i S^y_j - S^y_i S^x_j)$ is also included. On each bond, positive (negative) sign of D^z_{ij} is represented by $\odot$ ($\otimes$), and the direction from i- to j-site is indicated by the arrow. The tetrahedra CoO_4 on A- and B-sublattices are rotated around z axis with a rotation angle κ and $-\kappa$, respectively. See also Ref. [15]. (b) Magnetization curve for $\mathbf{B}^{\rm ex}\|x$. (c) EP along z-direction in the in-plane magnetic field $\mathbf{B}^{\rm ex} = (B^{\rm ex}\cos\phi_{\rm B}, B^{\rm ex}\sin\phi_{\rm B}, 0)$ ($B^{\rm ex} = 5$ T) on a 12-site cluster. Experimental data in (b) and (c) are extracted from Ref. 15 and Ref. 21, respectively.

splits single spin energies into two doubly degenerate states: $|\pm\frac{1}{2}\rangle$ with an eigenenergy $\Lambda/4$ and $|\pm\frac{3}{2}\rangle$ with $9\Lambda/4$. Here, $|m\rangle$ is a state with $S_z = m$ for spin $S = 3/2$. In the strong anisotropy limit $J/\Lambda \ll 1$, where we neglect the higher energy spin states $|\pm\frac{3}{2}\rangle$, an $S = 3/2$ Heisenberg model can be approximated by an XXZ model $\mathcal{H}^{\rm eff} = \sum J\{\Delta(\sigma^x_i\sigma^x_j + \sigma^y_i\sigma^y_j) + \sigma^z_i\sigma^z_j\}$ with $\Delta = 4$ by using an $S = 1/2$ spin operator σ [20]. It should be a good approximation to reproduce the lowest two branches of excitations. In fact, $\Delta \sim 2.5$ gives a good fit to neutron data in Ref. 16. On the other hand, the highest energy mode at 4 meV can be assigned to magnetic excitation due to the single ion anisotropy gap 2Λ.

To clarify the absorption processes at THz frequencies in detail, we investigate an $S = 3/2$ Heisenberg model on a square lattice with the uniaxial anisotropy term under external magnetic field $\mathbf{B}^{\rm ex}$:

$$\mathcal{H} = \sum_{n.n.}\left\{J\,\mathbf{S}_i\cdot\mathbf{S}_j - D^z_{ij}\,(S^x_i S^y_j - S^y_i S^x_j)\right\} + \sum\left\{\Lambda(S^z_i)^2 - g\mu_B\mathbf{B}^{\rm ex}\cdot\mathbf{S}_i\right\}, \quad (1)$$

where $\mathbf{S}_i$ is an $S = 3/2$ spin operator on i-site. The directions of Dzyaloshinsky-Moriya (DM) interactions D^z_{ij} on each bond can be determined uniquely from the crystal structure as in Fig. 1 (a) [22]. The DM interaction lifts the two-fold degeneracy in antiferromagnetic ordered states. Reflecting the rotation of CoO_4 tetrahedron around z axis, local EPs on i-site are given by $p^x_i = -K\,[\cos(2\kappa_i)(S^z_i S^x_i + S^x_i S^z_i) + \sin(2\kappa_i)(S^y_i S^z_i + S^z_i S^y_i)]$, $p^y_i = K\,[\cos(2\kappa_i)(S^y_i S^z_i + S^z_i S^y_i) + \sin(2\kappa_i)(S^z_i S^x_i + S^x_i S^z_i)]$, and $p^z_i = K\,[\cos(2\kappa_i)\{(S^y_i)^2 - (S^x_i)^2\} - \sin(2\kappa_i)(S^x_i S^y_i + S^y_i S^x_i)]$, where κ_i is the rotation angle with $\kappa_i = \kappa(-\kappa)$ on the $A(B)$-sublattice as in Fig. 1 (a) [15]. Magnetization and EP are defined as $M^\gamma = \sum g\mu_B\mu_0 S^\gamma_i$ and $P^\gamma = \sum p^\gamma_i$ ($\gamma = x, y$, and z), respectively. $\mathbf{M}$ and $\mathbf{P}$ under the in-plane external magnetic field $\mathbf{B}^{\rm ex}\|(\cos\phi_{\rm B}, \sin\phi_{\rm B}, 0)$ have been calculated by an exact diagonalization on N-site clusters ($N = 8, 10$, and 12). To reproduce M^x and P^z observed in Refs. 15 and 21, the parameters in Eq.(1) are estimated as $J/\Lambda = 0.125$, $|D^z|/\Lambda = 0.005$, $\Lambda = 1.3$ meV, $\kappa = \pi/8$, and $K = 3.8\times10^{-32}$ C·m. Here we use $g = 2$ while $V = 1.0\times10^{-28}$ m^3 is the volume per Co. As typical examples, the magnetization curve along $\mathbf{B}^{\rm ex}\|x$ and magnetic field direction dependence of P^z at $B^{\rm ex} = 5$ T on a 12-site cluster are shown in Figs. 1 (b) and (c), respectively. Here, system size effects are found to be negligibly small. Note that the magnon energy observed in the INS [16] at 2 K is also reproduced with this parameter set (see Fig. 2 (a)). We have confirmed that the results are qualitatively robust against choices of the parameters within the strong anisotropy limit $J/\Lambda \ll 1$.

Let us consider excitation processes by magnetic components of EMW, i.e., M1 transitions, which are related to the imaginary part of the magnetic susceptibility:

$$\mathrm{Im}\,\chi^{\rm mm}_{\gamma\gamma}(\omega) = \frac{\pi}{\hbar NV\mu_0}\sum_n |\langle n|M^\gamma|0\rangle|^2\,\delta(\omega-\omega_{n0}). \quad (2)$$

Here $|0\rangle$ is the ground state, $|n\rangle$ are excited states and $\hbar\omega_{n0}$ are excitation energies to $|n\rangle$ while $\gamma = x, y$, and z. Eq. (2) is calculated on N-site clusters ($N = 8, 10$, and 12) by the Lanczos method [23], where the δ-function is replaced by a Lorentzian with a width $\epsilon/\Lambda = 0.1$. The results at $B^{\rm ex} = 0$ are shown in Fig. 2 (a). Out of plane component $\mathrm{Im}\,\chi^{\rm mm}_{zz}(\omega)$ vanishes. In-plane components are found to be identical, $\mathrm{Im}\,\chi^{\rm mm}_{yy}(\omega) = \mathrm{Im}\,\chi^{\rm mm}_{xx}(\omega)$. They show that the magnetic components H^ω_x and H^ω_y induce magnetic resonances at around 2 meV and 4 meV (Fig. 2 (a)). As shown in the figure, the system size effects are small. Hereafter, we show the results on the 12-site cluster. We indeed see that the excitation around 2 meV corresponds to one of the spin-wave branches observed in the INS [16], while the higher energy mode is an excitation accompanied with the anisotropy gap excitation 2Λ. These features are clarified from J dependence of the peak positions. As shown in the inset of Fig. 2 (a), in decreasing J, the high energy peak continuously shifts to single site gap excitation $2\Lambda = 2.6$ meV, whereas the low energy peak position is proportional to J.

When spin states couple to electric fields through EP, E1 process may excite magnetic excitations [24, 25]. Such processes can be clarified from the dielectric susceptibility via spin-dependent EP

$$\mathrm{Im}\,\chi^{\rm ee}_{\gamma\gamma}(\omega) = \frac{\pi}{\hbar NV\epsilon_0}\sum_n |\langle n|P^\gamma|0\rangle|^2\,\delta(\omega-\omega_{n0}). \quad (3)$$

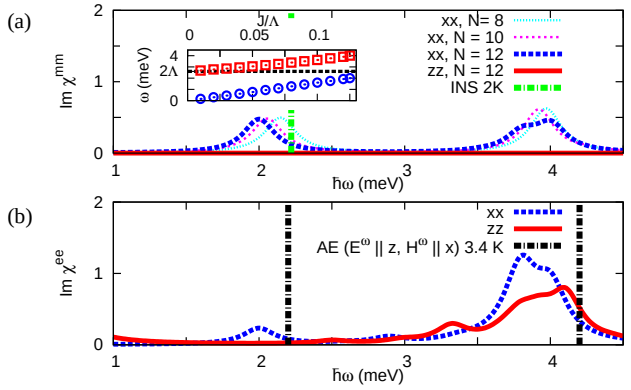

FIG. 2: (Color online) (a) Im $\chi^{\rm mm}_{\gamma\gamma}(\omega)$ for $\gamma = x$, and z. Magnon energy observed in INS is extracted from Ref. 16. Inset: Peak positions around 2 and 4 meV for Im $\chi^{\rm mm}_{xx}(\omega)$ as a function of J/Λ on 12-site cluster. (b) Im $\chi^{\rm ee}_{\gamma\gamma}(\omega)$ for $\gamma = x$, and z on 12-site cluster. Peak positions observed in THz AE for E^ω_z and H^ω_x polarizations are extracted from Ref. 19.

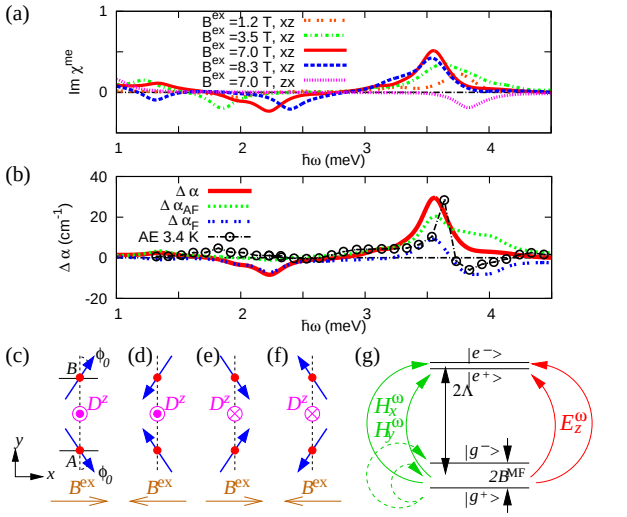

FIG. 3: (Color online) (a) Im $\chi^{\rm me}_{xz}(\omega)$ under the external magnetic fields $\mathbf{B}^{\rm ex}\|x$. At 7 T, Im $\chi^{\rm me}_{zx}(\omega)$ is also shown. (b) Difference of the absorption coefficient by EMW propagating directions $\Delta\alpha(\omega)$ at $B^{\rm ex}_x = 7$ T, which can be decomposed to ferromagnetic component $\Delta\alpha_{\rm F}(\omega)$ and antiferromagnetic one $\Delta\alpha_{\rm AF}(\omega)$. $\Delta\alpha(\omega)$ obtained from THz AE for E^ω_z and H^ω_x are extracted from Ref. 19. (c)-(f) Two sublattice spin structures in $B^{\rm ex}_x$. See text for detail. (g) Excitation process in the limit $B^{\rm MF}/\Lambda \ll 1$.

At $B^{\rm ex} = 0$, in-plane components of dielectric susceptibility are found to be uniform, $\mathrm{Im}\,\chi^{\rm ee}_{yy}(\omega) = \mathrm{Im}\,\chi^{\rm ee}_{xx}(\omega)$, as in the case for the magnetic susceptibility. Contributions to the 2 meV absorption are small. The 4 meV resonance is active for any electric components (see Fig. 2 (b)). From these results, we conclude that the selection rules and the peak positions are consistent with those obtained in the THz AE [19].

The temperature dependence of THz AE can also be explained qualitatively. In Ref. 19, 4 meV absorption is observed even above T_N, whereas absorption at 2 meV vanishes at T_N upon increasing the temperature. The anisotropy gap excitation energy $2\Lambda \sim 30$ K is larger than T_N, and such a resonance can be observed even above Néel temperature, i.e., $T_N < T \lesssim 2\Lambda$. However, the resonance at 2 meV vanishes above T_N, since the spin wave excitation exists only in the ordered state.

In practice, M1 and E1 processes are invoked through the interaction with EMW as $\mathcal{H}' = -\mathbf{E}^\omega \cdot \mathbf{P} - \mathbf{H}^\omega \cdot \mathbf{M}$, where $\mathbf{E}^\omega$ ($\mathbf{H}^\omega$) is the electric (magnetic) component of EMW. Provided that both M1 and E1 processes induce an identical excitation, there is a cross correlation between magnetic and electric components of EMW, i.e., the interference between electric and magnetic responses. As we show details in the following, the effects of the interference can be observed directly as the linear NDD, e.g., the interference enhances absorption intensity for the EMW with a propagation vector $+\mathbf{k}$ but weakens that for the EMW with $-\mathbf{k}$, since reversing $\mathbf{k}$ is equivalent to reversing the relative sign of $\mathbf{E}^\omega$ and $\mathbf{H}^\omega$ due to $\mathbf{H}^\omega = (1/\mu_0\omega)\mathbf{k} \times \mathbf{E}^\omega$. As a typical case, we consider dynamical magnetoelectric susceptibility for M^x and P^z

$$\mathrm{Im}\chi^{\rm me}_{xz}(\omega) = \sum_n \frac{\pi c}{2\hbar NV}\Big(\langle 0|M^x|n\rangle\langle n|P^z|0\rangle$$

$$+\langle 0|P^z|n\rangle\langle n|M^x|0\rangle\Big)\,\delta(\omega-\omega_{n0}), \quad (4)$$

where $c \equiv 1/\sqrt{\epsilon_0\mu_0}$. The results under $\mathbf{B}^{\rm ex}\|x$ are shown in Fig. 3 (a). $\mathrm{Im}\chi^{\rm me}_{xz}(\omega)$ is enhanced around 4 meV excitation. Note that $\mathrm{Im}\chi^{\rm me}_{zx}(\omega)$ is much smaller than $\mathrm{Im}\chi^{\rm me}_{xz}(\omega)$. $\mathrm{Im}\chi^{\rm me}_{zx}(\omega)$ at 7 T is also shown in Fig. 3 (a).

Experimentally, such a cross correlated effect can be observed as the linear NDD [19]. By introducing a complex refractive index N, a polarized plane wave with $\mathbf{E}^\omega\|z$, $\mathbf{H}^\omega\|x$ and $\mathbf{k}\|y$ is described as $E^\omega_z = E^z_0\exp(-i\omega(t-(Ny/c)))$ and $H^\omega_x = H^x_0\exp(-i\omega(t-(Ny/c)))$. From the Maxwell's equations, N is given as $N^\pm \sim \sqrt{\epsilon_{zz}(\omega)\mu_{xx}(\omega)} \pm \chi^{\rm me}_{xz}(\omega)$ where $\mu_{xx}(\omega) = 1+\chi^{\rm mm}_{xx}(\omega)$ and $\epsilon_{zz}(\omega) = 1+\chi^{\rm ee}_{zz}(\omega)$. Here, N^+ (N^-) is a complex refractive index for EMW propagating to $+y$ ($-y$) direction. Thus, non-reciprocal part of an absorption coefficient $\alpha^\pm(\omega) = (\omega/c)\,\mathrm{Im}N^\pm$ is given by $\Delta\alpha(\omega) = \alpha^+(\omega) - \alpha^-(\omega) = (2\omega/c)\,\mathrm{Im}\chi^{\rm me}_{xz}(\omega)$. $\Delta\alpha(\omega)$ at $B^{\rm ex}_x = 7$ T is shown in Fig. 3 (b), where the peak position and the magnitude of $\Delta\alpha(\omega)$ are consistent with those observed in THz AE [19].

Let us consider the magnetic origin for non-reciprocal part of the absorption coefficient $\Delta\alpha(\omega) \sim (2\omega/c)\,\mathrm{Im}\chi^{\rm me}_{xz}(\omega)$. Under the external magnetic field $\mathbf{B}^{\rm ex} \perp z$, spin structure in the Néel ordered state is uniquely determined due to an energy gain of the DM term, e.g., the state in Fig. 3 (c) is stabilized by $\mathbf{B}^{\rm ex}\|x$ with $B^{\rm ex}_x > 0$. The EMW propagating to $-y$ direction

in Fig. 3 (c) corresponds to that propagating to $+y$ direction in Fig. 3 (d) which is realized by a 180° rotation around z axis on a spin site. Thus, reversing the magnetic field $B_x^{\rm ex} \to -B_x^{\rm ex}$ is equivalent to reversing the EMW direction $k^y \to -k^y$, which is consistent with the experimental observation [19]. Note that, when we reverse the magnetic field $B_x^{\rm ex} \to -B_x^{\rm ex}$, both ferromagnetic moment $m_u^x \equiv S_A^x + S_B^x$ and antiferromagnetic component $m_s^y \equiv S_A^y - S_B^y$ change their sign as shown in Figs. 3 (c) and (d). Each contribution to $\Delta\alpha(\omega)$ can be obtained by changing the sign of D^z in the calculation, since only m_s^y (m_u^x) changes its sign between states in Figs. 3 (c) and (e) ((c) and (f)). As a result, $\Delta\alpha(\omega)$ is decomposed into two parts $\Delta\alpha_{\rm F}(\omega)$ and $\Delta\alpha_{\rm AF}(\omega)$, which depend on the modification of m_u^x and m_s^y, respectively. By comparing absorptions for the states in Figs 3 (c)-(f), $\Delta\alpha_F(\omega)$ and $\Delta\alpha_{\rm AF}(\omega)$ are extracted as in Fig. 3 (b). The results indicate that $\Delta\alpha_{\rm AF}(\omega)$ is dominant for the NDD around 4 meV. Generally, NDD can be realized when spontaneous magnetization and EP coexist. In the present model, however, realization of a Néel ordered state without ferromagnetic moment is sufficient to induce NDD. Once a single domain structure of the Néel ordered state is realized, $\Delta\alpha(\omega)$ can be finite even at $B_x^{\rm ex} \to 0$ and $|D_{ij}^z| \to 0$.

Finally, we note that the selection rules and the cross correlated effects can qualitatively be determined within a mean field (MF) approximation. The spin Hamiltonian (1) can be approximated as $\mathcal{H}^{\rm MF} = \sum\{\Lambda(S_i^z)^2 - g\mu_B \mathbf{B}_i^{\rm MF}\cdot\mathbf{S}_i\}$, where $g\mu_B\mathbf{B}_i^{\rm MF} \equiv g\mu_B\mathbf{B}^{\rm ex} - \sum_j\{J\langle\mathbf{S}_j\rangle \mp |D_{ij}^z|(\langle S_j^y\rangle, -\langle S_j^x\rangle, 0)\}$ (−(+) for the i-site on $A(B)$-sublattice). For simplicity, spin states under $\mathbf{B}_i^{\rm MF} = (B^{\rm MF}\cos\phi_i, B^{\rm MF}\sin\phi_i, 0)$ in the limit $B^{\rm MF}/\Lambda \ll 1$ are discussed. Four eigenstates at site i are given in a form: $|g_i^{\pm}\rangle = \frac{1}{\sqrt{2}}(e^{-i\phi_i/2}|\frac{1}{2}\rangle \pm e^{i\phi_i/2}|-\frac{1}{2}\rangle)$ and $|e_i^{\pm}\rangle = \frac{1}{\sqrt{2}}(e^{-i3\phi_i/2}|\frac{3}{2}\rangle \pm e^{i3\phi_i/2}|-\frac{3}{2}\rangle)$ as in Fig. 3 (g). Eigenenergies for $|g_i^{\pm}\rangle$ are $\Lambda/4 \mp g\mu_B B^{\rm MF}$ and for both $|e_i^{\pm}\rangle$, $9\Lambda/4$. As a typical example, let us consider excitation processes induced by H_x^ω, H_y^ω and E_z^ω. From the ground state $|g_i^+\rangle$, processes through S_i^x, S_i^y and p_i^z are

$$\begin{aligned} S_i^x|g_i^+\rangle &= \cos\phi_i|g_i^+\rangle + i\sin\phi_i|g_i^-\rangle \\ &\quad +\sqrt{3}(\cos\phi_i|e_i^+\rangle + i\sin\phi_i|e_i^-\rangle)/2, \quad (5) \\ S_i^y|g_i^+\rangle &= \sin\phi_i|g_i^+\rangle - i\cos\phi_i|g_i^-\rangle \\ &\quad +\sqrt{3}(\sin\phi_i|e_i^+\rangle - i\cos\phi_i|e_i^-\rangle)/2, \quad (6) \\ p_i^z|g_i^+\rangle &= -\sqrt{3}K\cos(2\phi_i - 2\kappa_i)|e_i^+\rangle \\ &\quad -i\sqrt{3}K\sin(2\phi_i - 2\kappa_i)|e_i^-\rangle. \quad (7) \end{aligned}$$

We see that E_z^ω can only induce magnetic excitations with the anisotropy gap 2Λ. This is consistent with the results in Fig. 2 (b). For the EMW with $\mathbf{E}^\omega \| z$ and $\mathbf{H}^\omega \| (\cos\phi_\omega, \sin\phi_\omega, 0)$, the cross correlation effect is qualified by a spectral weight $\Delta I(\phi^\omega) \propto \int(\cos\phi_\omega {\rm Im}\chi_{xz}^{\rm me}(\omega) + \sin\phi_\omega {\rm Im}\chi_{yz}^{\rm me}(\omega))d\omega$. The canted Néel ordered state under $\mathbf{B}^{\rm ex} \| (\cos\phi_{\rm B}, \sin\phi_{\rm B}, 0)$ gives $\phi_i = \phi_{\rm B} \mp (\pi/2 - \phi_0)$ (−(+) for the spin on $A(B)$-sublattice), where ϕ_0 is a spin canting angle. By applying Eqs. (5)-(7) to Eq. (4), we obtain that

$$\Delta I(\phi_\omega) \propto \cos(\phi_\omega + \phi_{\rm B})\sin(2\kappa - \phi_0). \quad (8)$$

For $\phi_{\rm B} = 0$ (a state in Fig. 3 (c)), we obtain that $\Delta I(0) \propto \sin(\phi_0 - 2\kappa)$ (for $\mathbf{H}^\omega \| x$) and $\Delta I(\pi/2) = 0$ (for $\mathbf{H}^\omega \| y$) as already expected from the symmetry argument in Ref. 19. We see $\Delta I(0) \neq 0$ even for $\phi_0 = 0$, which indicates the existence of the NDD in a collinear Néel ordered state.

In addition, we can predict the NDD for $\mathbf{k}\|[010]$, $\mathbf{E}^\omega\|[001]$, and $\mathbf{H}^\omega\|[100]$ ($\phi_\omega = -\pi/4$) under $\mathbf{B}^{\rm ex}\|[010]$ ($\phi_{\rm B} = \pi/4$), although there is no spontaneous EP [15] for this $\mathbf{B}^{\rm ex}$ direction. In fact, $\chi_{[100][001]}^{\rm me}(\omega)$ under $\mathbf{B}^{\rm ex}\|[010]$ is found to be non-zero in the numerical calculation. Observation of the NDD in this condition is a crucial test for the validity of our theory. As another example, we can easily derive $\Delta I_{zx} \propto \int {\rm Im}\chi_{zx}^{\rm me}(\omega)d\omega = 0$ for the EMW with $\mathbf{E}^\omega \| x$ and $\mathbf{H}^\omega \| z$ under $\mathbf{B}^{ex} \| x$, which is consistent with the results calculated at $B_x^{\rm ex} = 7$ T: $\int {\rm Im}\chi_{zx}^{\rm me}(\omega)d\omega \ll \int {\rm Im}\chi_{xz}^{\rm me}(\omega)d\omega$ (see Fig. 3 (a)).

Our results indicate the potential of the spin-dependent metal-ligand hybridization mechanism for novel absorption processes which might be observed in a wide range of materials with a spin at a site without inversion center, e.g., in a tetrahedron and a pyramid of ligand atoms.

We thank I. Kézsmárki, N. Kida, S. Bordács H. Murakawa, Y. Onose, T. Arima, R. Shimano, and Y. Tokura for fruitful discussion. This work is in part supported by Grant-In-Aids for Scientific Research from the Ministry of Education, Culture, Sports, Science and Technology (MEXT) Japan.

[1] Y. Tokura, Science **312**, 1481 (2006).
[2] W. Eerenstein et al., Nature (London) **442**, 759 (2006).
[3] S.-W. Cheong and M. Mostovoy, Nat. Mater. **6**, 13 (2007).
[4] T. Kimura et al., Nature (London) **426**, 55 (2003).
[5] A. Pimenov et al., Nat. Phys. **2**, 97 (2006).
[6] N. Kida et al., J. Opt. Soc. Am. B **26**, A35 (2009).
[7] R. V. Aguilar et al., Phys. Rev. Lett. **102**, 047203 (2009).
[8] S. Seki et al., Phys. Rev. Lett. **105**, 097207 (2010).
[9] T. Arima et al., Phys. Rev. Lett. **96**, 097202 (2006).
[10] H. Katsura et al., Phys. Rev. Lett. **95**, 057205 (2005).
[11] M. Mostovoy, Phys. Rev. Lett. **96**, 067601 (2006).
[12] I. A. Sergienko and E. Dagotto, Phys. Rev. B **73**, 094434 (2006).
[13] C. Jia et al., Phys. Rev. B **74**, 224444 (2006).
[14] T. Arima, J. Phys. Soc. Japan **76**, 073702 (2007).
[15] H. Murakawa et al., Phys. Rev. Lett. **105**, 137202 (2010).
[16] A. Zheludev et al., Phys. Rev. B **68**, 024428 (2003).
[17] H. T. Yi et al., Appl. Phys. Letter **92**, 212904 (2008).
[18] I. Kézsmárki et al. (2011), private communication.

[19] I. Kézsmárki et al. (2010), accepted for publication in Phys. Rev. Lett. (e-print available at arXiv:1010.5420).
[20] p^z is suppressed as $B_x^{\rm ex}$ is decreased below $\sim$ 1 T and deviates from the theoretical estimates based on a classical spin picture [15]. However, the suppression of p^z at $B_x^{\rm ex} = 0$ can be understood by considering the effects of quantum fluctuation in a limit $\Lambda \to \infty$ on a single site, since $\langle p^z \rangle$ vanishes for any linear combinations of $|\pm\frac{1}{2}\rangle$.
[21] H. Murakawa, Y. Onose, and Y. Tokura (2010), unpbulished.
[22] D^x (D^y) component on the bond along y (x) direction is also non-zero, but the effects of them are found to be negligible in the calculations.
[23] E. Dagotto, Rev. Mod. Phys. **66**, 763 (1994).
[24] Y. Tanabe et al., Phys. Rev. Lett. **15**, 1023 (1965).
[25] H. Katsura et al., Phys. Rev. Lett. **98**, 027203 (2007).